August 1, 1999

Equatorial and low latitude thermospheric winds: Measured quiet time variations with season and solar flux from 1980 to 1990

M. A. Biondi
S. Y. Sazykin
Bela G. Fejer, *Utah State University*
J. W. Meriwether
C. G. Fesen

JOURNAL OF GEOPHYSICAL RESEARCH, VOL. 104, NO. A8, PAGES 17,091-17,106, AUGUST 1, 1999

Equatorial and low latitude thermospheric winds: Measured quiet time variations with season and solar flux from 1980 to 1990

M. A. Biondi,[1] S. Y. Sazykin,[2] B. G. Fejer,[2] J. W. Meriwether,[3] and C. G. Fesen[4]

Abstract. Thermospheric winds have been systematically determined at Arequipa, Peru, and Arecibo, Puerto Rico, from Fabry-Perot interferometer measurements of Doppler shifts in the nightglow 630 nm line. The wind databases (1983 - 1990 at Arequipa and 1980 - 1990 at Arecibo) have been edited to eliminate measurements during geomagnetically disturbed conditions, then sorted by season and solar flux level. Following this, they were averaged to obtain the climatological behavior of the nighttime wind variations at the two locations. A new averaging technique, multivariate regression analysis, has been applied to the data, and the results compared to our prior binning averages. The observed wind behaviors at the Arequipa and Arecibo Observatories, which are at equal geographic latitudes on opposite sides of the equator, are contrasted to establish the seasonal flow patterns. The regression analysis results have then been compared with the predicted behavior provided by the National Center for Atmospheric Research's Thermosphere-Ionosphere-Electrodynamics General Circulation Model. In many cases, qualitative agreement between measurements and predictions is found as to wind directions and temporal variations, with differences in magnitude of ~0-50 m/s. However, some striking differences are found that may arise from ionosphere-thermosphere coupling effects. The overall results provide an important step in establishing the climatology of the thermospheric winds at equatorial and low-latitude sites.

1. Introduction

The observed behaviors of the nighttime equatorial thermospheric neutral winds and temperatures have been described in several papers [*Biondi and Meriwether*, 1985; *Meriwether et al.*, 1985, 1986; *Biondi et al.*, 1990, 1991; *Meriwether and Biondi*, 1995; *Meriwether et al.*, 1996,1997], based on ground-based Fabry-Perot interferometer (FPI) measurements from Arequipa, Peru (16.5°S, 71.5°W, 3.2°S dip latitude) since 1983. Inasmuch as the thermospheric "weather" exhibits large day-to-day variations, extraction of seasonal and solar cycle variations ("climate") from the measurements requires development and use of suitable averaging techniques to suppress the day-to-day variability. In the two earlier thermospheric wind papers dealing with seasonal and solar cycle variations [*Biondi et al.*, 1990, 1991], data for a given month/year were sorted into 30 min time bins during the night and averaged to obtain point-by-point average values and standard deviations that represented the nocturnal variations for a given month. This procedure suppressed much of the weather variations and gave some insight into the thermospheric wind's climate. However, the sorting of the data into given month/year segments led to relatively few data points per bin and consequently substantial statistical uncertainties in the average wind values.

The purpose of the present paper is to obtain a better understanding of the climatology through the use of improved data analysis techniques. To this end, the raw wind data from Arequipa have first been reanalyzed using slight modifications of the bin-averaging techniques to provide a baseline for comparison (all of the wind graphs in this paper have been corrected for the scale factor error in the 1988-1990 graphs of *Biondi et al.* [1990, 1991]). Following this, a rather sophisticated averaging technique, multivariate local regression analysis, has been introduced to treat the data. This method offers distinct advantages over the earlier procedures, providing a description of the thermospheric meridional and zonal wind fields as functions of S_a, the solar flux index, and t, the time during the night.

In addition, the FPI database of similar measurements during 1980-1990 from Arecibo, Puerto Rico (18.6°N, 66.8°W, 29°N dip latitude) [*Burnside et al.*, 1981], has been analyzed in like fashion. This affords us an opportunity to compare the thermospheric wind behaviors at these two observatories "mirrored" in geographic latitude across the equator but at quite different geomagnetic latitudes.

The present results summarize data obtained at the two low-latitude sites over extended time periods. They therefore complement the information obtained from the Dynamics Explorer and Atmospheric Explorer series of satellite-borne FPIs [e.g., *Hedin et al.*, 1988, 1991 and references therein], which provide much broader global coverage but poorer determinations of local time variations. Also, to test the predictions of sophisticated models against our measured thermospheric wind behaviors, we have included appropriate results obtained from the National Center for Atmospheric Research (NCAR) Thermosphere-Ionosphere-Electrodynamics General Circulation Model (TIEGCM) for comparison.

[1]Department of Physics and Astronomy, University of Pittsburgh, Pittsburgh, Pennsylvania.
[2]Center for Atmospheric and Space Sciences, Utah State University, Logan.
[3]Department of Physics and Astronomy, Clemson University, Clemson, South Carolina.
[4]W B Hanson Center for Space Sciences, University of Texas, Dallas, Richardson.

Paper number 1999JA900174.
0148-0227/99/1999JA900174$09.00

2. Data Acquisition and Analysis Techniques

The nighttime thermospheric winds and temperatures over Arequipa and Arecibo are determined by use of large-aperture FPIs observing the OI 630 nm nightglow radiation to determine the Doppler shifts and widths in the emitted line. The field-widened 100 mm aperture Arequipa instrument and the 150 mm aperture Arecibo instrument have comparable sensitivities and have been described in a number of publications [e.g., *Burnside et al.*, 1981; *Biondi and Sipler*, 1985; *Biondi and Meriwether*, 1985; *Meriwether et al.*, 1997]. The measured Doppler shifts in the 630 nm nightglow OI line for observations along several azimuths at 60^0 zenith angle and in the zenith have been used to determine the corresponding line-of-sight (los) velocities. From these shifts the meridional and zonal components of the thermospheric wind are inferred as a function of time during the night [*Burnside et al.*, 1981; *Biondi et al.*, 1990, 1991]. Examples of these point-by-point measurements for a number of nights at Arequipa and Arecibo are illustrated by the scatterplots in the lower portion of each frame of Figure 1, indicating the substantial variations, both point-to-point and night-to-night. (In all of the figures, northward meridional and eastward zonal winds are taken as positive.)

In order to present the climatological behaviors of the meridional and zonal thermospheric wind components via suitable averages, we have assumed that, for measurements during geomagnetically quiet periods, the factors controlling the ther mospheric circulation are the solar EUV flux, the location of the subsolar point, and the rotation of Earth, i.e., local time

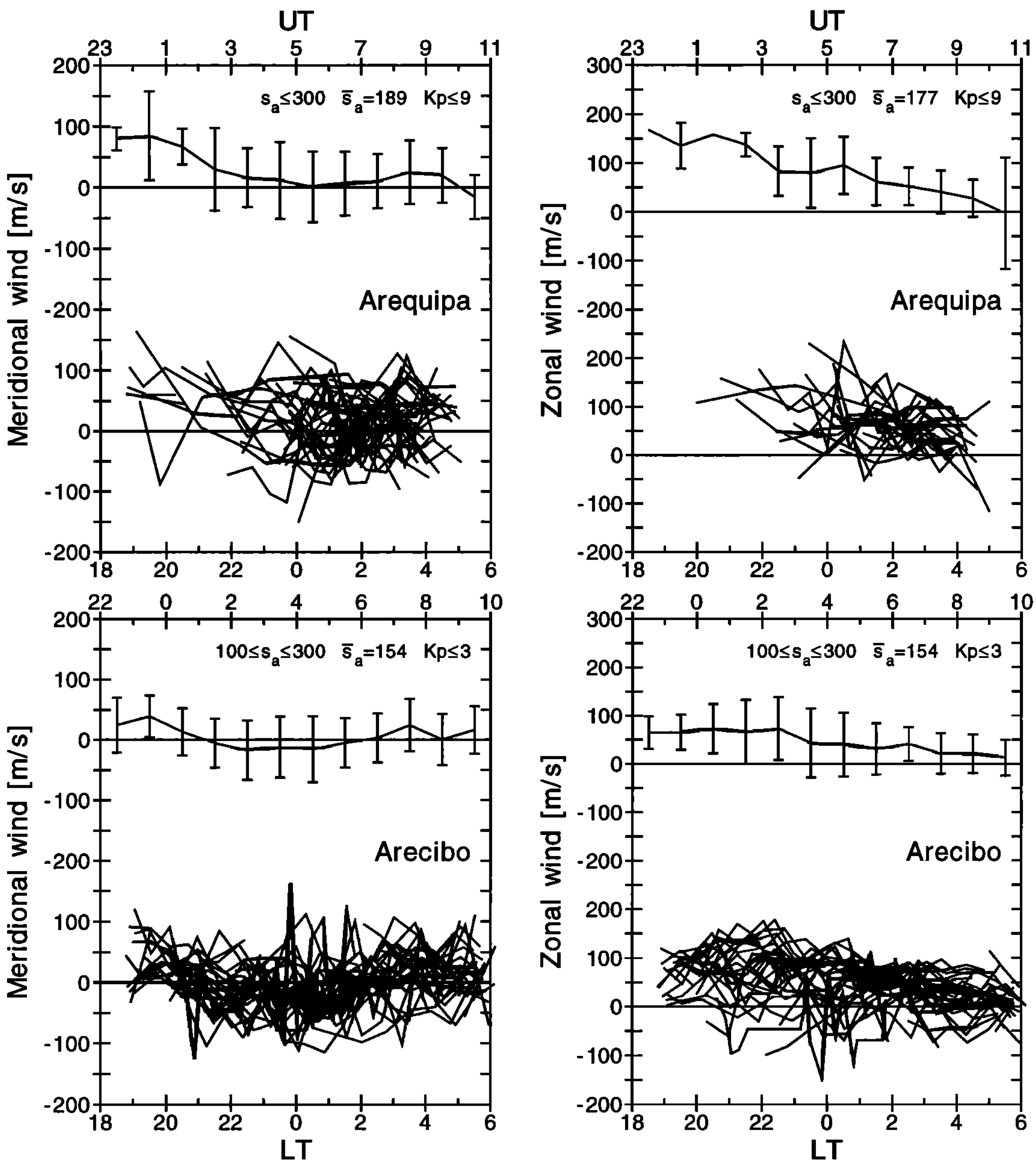

Figure 1. Thermospheric wind components at Arequipa and Arecibo during the November - February solstice period. In all figures, northward and eastward wind components are taken as positive. Lower portions of the panels show scatterplots of the measured nightly winds, indicating the large night-to-night variations. In the upper portions of the panels, straight-line segments connect hourly bin average values, while the vertical symbols indicate the $\pm 1\sigma$ limits of the variations.

variations. (We have not taken into account two additional quiet time seasonal factors, the sporadic effect on the winds of gravity wave dissipation [*Meriwether et al.*, 1996, 1997] and the varying ion drag from the thermosphere-ionosphere interaction, see, e.g., the overview by *Fejer* [1997].) In most cases the observed wind behaviors appear to support these assumptions. Thus the average wind patterns and strengths should be functions mainly of season and solar activity, represented by the indices $F_{10.7}$ or S_a. (Note that we have used the actual solar flux index $F_{10.7}$ and the normalized (to 1 AU) S_a value interchangeably, since the two differ by ~3 % or less.) The effects of geomagnetic activity (storms) on the circulation are minimized by selecting data for which *Kp* is low during the time of measurement.

To implement these assumptions, we have selected those nocturnal wind data sets taken under geomagnetically quiet conditions (i.e., $Kp \leq 3$, with one exception), then sorted them by S_a, which represents the solar flux, and by season (groups of months), without regard to the year in which the measurements were made. This is a departure from the earlier work [*Biondi et al.*, 1990, 1991], where monthly averages were presented for each year. This modified procedure follows from our finding that, for quiet geomagnetic conditions, the behavior in particular seasons (the equinoxes taken together and the summer and the winter solstices) is characterized not by the month/year but chiefly by the solar flux level.

2.1. Bin Averaging

One way to display the average behavior of the winds over a given period is to sort the data for the appropriate set of nights into 1 hour time bins (in the earlier papers, 30 min bins were used) and then average to produce the results shown in the upper portion of each of the frames within Figure 1. The solid lines pass through the mean values, and the vertical bars indicate the $\pm 1\sigma$ limits of the night-to-night variations in wind values in the given time bin (the measurement errors are smaller, typically ± 20 m/s). A variation on this bin-averaging scheme is illustrated in Figures 2 and 3. Since the winds should vary smoothly with time in describing the climatology for geomagnetically quiet conditions, a Gaussian filter (three-point running weighted average) has been applied to the average wind values for each time bin, thereby smoothing the curves.

2.2. Multivariate Regression Analysis

A new method of data analysis has been introduced in order to provide a better representation of the dependence of the winds on solar flux level and local time than has been obtained with the previous averaging techniques. The approach involves use of fitting via local regression [*Cleveland*, 1979; *Cleveland and Devlin*, 1988; *Cleveland et al.*, 1988] to estimate a regression surface in two dimensions. Only a brief description of the technique will be given; the method is discussed in detail by *Cleveland et al.* [1988].

We assume that our dependent variable v (which can be either component of the horizontal wind) under geomagnetically quiet conditions is a function of two independent variables S_a and t (local time). Given that our data points are randomly distributed in the S_a- t plane, we wish to obtain the best possible determination

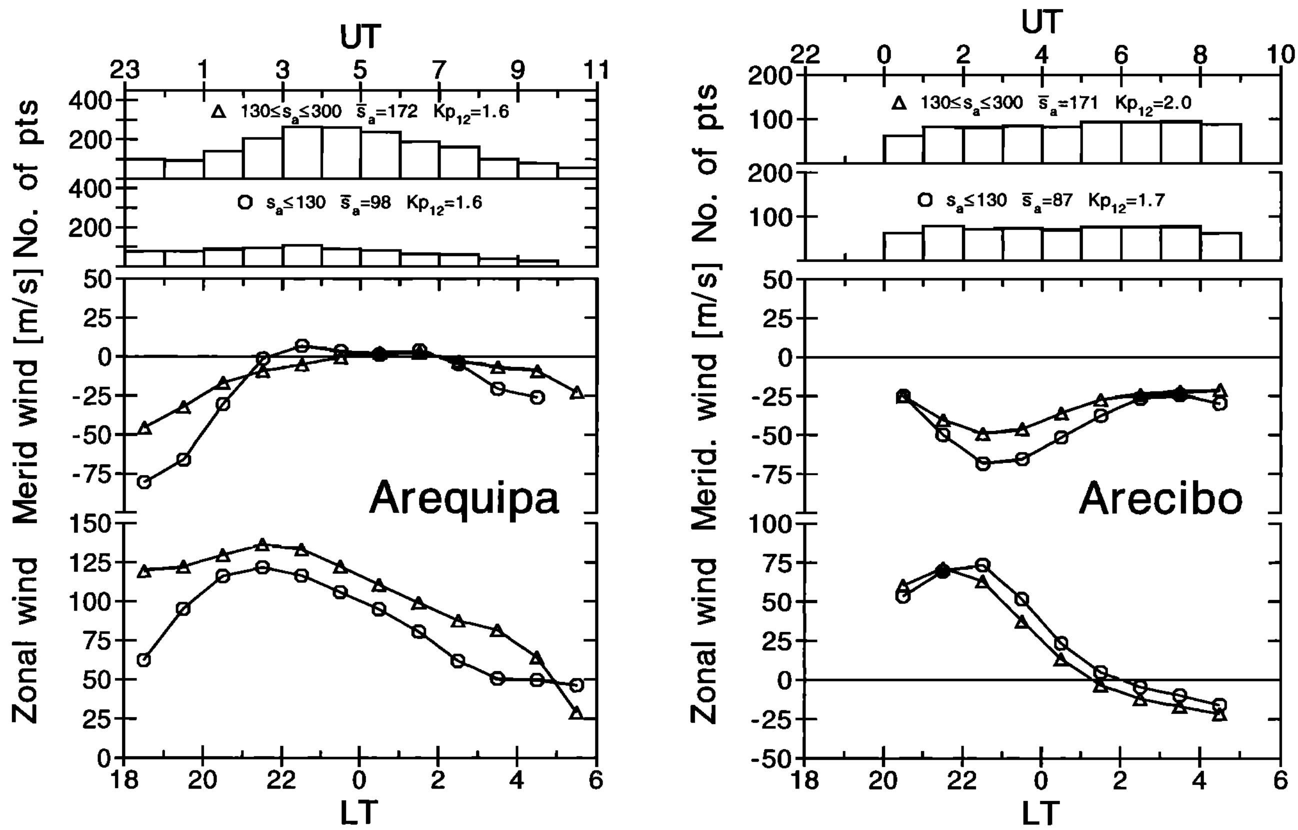

Figure 2 Thermospheric wind components during the May - August solstice for $Kp \leq 3$ for Arequipa 1983-1990 and Arecibo 1980-1990. Top panels show number of data points in each 1-hour bin. In the lower panels, points indicate three-point running weighted averages of the binned values: circles, average solar flux 87 or 98; triangles, 171 or 172.

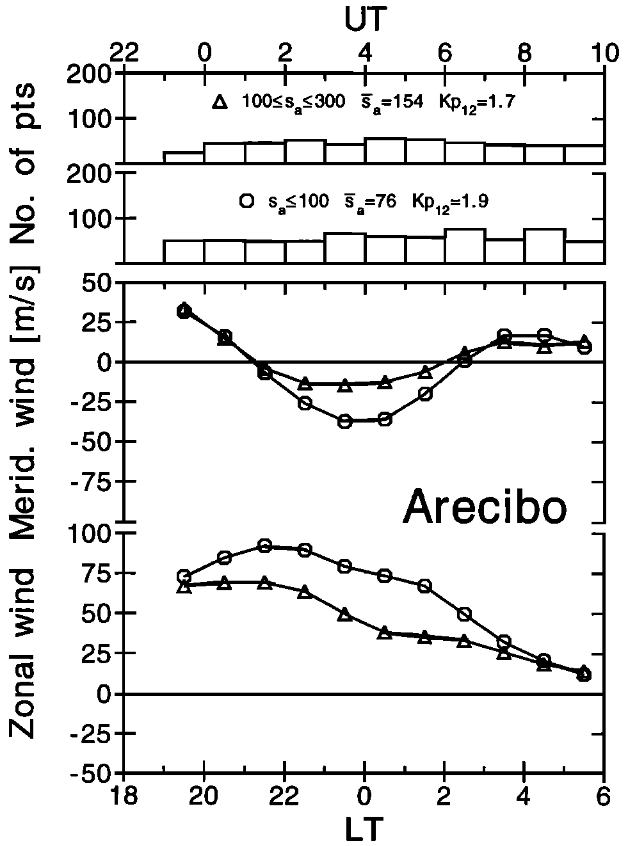

Figure 3. Same format as in Figure 2. November - February solstice (Arecibo winter) 1980-1990 for $Kp \leq 3$. but average solar fluxes are: circles, 76; triangles, 154.

of the surface $v = v(S_a, t)$ from a limited number of measurements. Regression surfaces are fitted to data through multivariate smoothing in a moving fashion conceptually similar to how a moving average is computed for a time series. Let v^i $(i = 1, ..., n)$ be measurements of a wind component, and S_a^i and t^i the values of the independent variables. It is assumed that $v^i = g(S_a^i, t^i) + E^i$, where g is the true dependence of v on S_a and t, and E^i are residuals that are themselves independent normal variables with mean 0 and variance σ^2. Instead of making the usual assumption that g is some parametric function (e.g., a combination of polynomials), we only assume that g is a smooth function of S_a and t. This allows us to choose g from a larger class of functions and avoid distortions of g characteristic of global parametric fitting.

The concept of local regression can be summarized as follows: to estimate g at an arbitrary point (S_a^0, t^0) we select a neighborhood of q points that are closest to (S_a^0, t^0), as measured by the usual (Euclidean) distance $[(S_a^i - S_a^0)^2 + (t^i - t^0)^2]^{1/2}$ in the S_a - t plane (the distances in S_a and t are normalized to their variances, since they have different units). The q points are weighted according to the distance of (S_a^i, t^i) from (S_a^0, t^0); a linear polynomial in two dimensions is then fitted by weighted least squares, and the value of that polynomial at (S_a^0, t^0) is taken as the value of the fitted function at that point. For practical purposes, since regression surfaces are smooth, it is sufficient to carry out the procedure for a number of points covering the region ($70 \leq S_a \leq 200$; $1800 \leq t \leq 0600$ LT) and forming a 50x50 point uniform grid. Around each grid point a circle is drawn to encompass a fixed fraction α of the total number of points n to yield the desired value of q. To eliminate possible deviant points, the values of v in the circle are sorted, and the 10% of the points with the lowest and the highest values are deleted. For the remaining points, weights are assigned that vary inversely with the distance from the center of the circle, and a least squares fit is perfomed, as described above.

The smoothness of the regression surface is controlled by the parameter α that has been chosen empirically, with larger values of α yielding smoother surfaces. Since the estimates of the surface g at the grid points are linear combinations of the measurements of v^i in that circle, distributional results for local regression are the same as for the usual least squares. Statistical quantities can be defined for local regression in analogy with least squares [*Cleveland et al.*, 1988]; therefore, in the subsequent discussion of both bin average plots and regression surfaces, we have introduced the quantity σ, the (equivalent) standard error. For bin averages it is the square root of the variance, while for regression analysis it is the square root of the variance of the residuals [see *Cleveland et al.*, 1988]. The quantity σ reflects chiefly the large point-to-point variability in the measured winds, since the uncertainties in the Doppler shift determinations are usually significantly smaller.

Since the values of σ computed for our regression surfaces are typically large, questions occur concerning how significant are the apparent variations in the deduced winds. This is related to whether the appropriate value of the smoothing parameter α has been chosen; if α is too small, "noisy" surfaces reproducing the data's variability result; if α is too large, the result is very smooth surfaces with little variability. Although the usual goodness-of-fit statistical tests cannot be defined for nonparametric fitting methods such as were used in the present work, we have used an alternative approach, an analysis-of-variance, as a test of the significance of the variations of the winds deduced from the regression analysis.

First, we chose values of α meeting the requirement that the resultant residuals contained little variability. As the next step, for each surface a larger value of α was chosen, and the surface recomputed (yielding less variability). We then performed an analysis-of-variance to see if the new surface did indeed give a better fit to the data. The appropriate test statistic (for the exact definition, see *Cleveland et al.*[1988]) measures the reduction in σ and has an F-distribution with numerator and denominator degrees of freedom found from the local regression properties. For all fits, we chose values of α so that the fits are significant within 5% confidence levels (provided that the assumptions for the validity of such a test hold).

The results of the regression analysis are given in Figures 4, 5, and 6 in the same form of data presentation as used previously. The more complete descriptions of the wind-component contours in the S_a - t plane are shown in Figures 7, 9, and 11. In both figure formats, linear interpolation is used between the calculated points. In Figure 7, the local time (LT) extents for Arequipa and Arecibo differ owing to the different lengths of the nighttime observing periods at the two observatories.

3. Model Wind Calculations

The thermospheric winds deduced from the data are compared with predictions from the TIEGCM, most recently described by *Richmond et al.* [1992 and references therein]. The runs used here all assume low geomagnetic activity, corresponding to a cross-polar-cap potential of 40 kV in the model. The O^+-O collision frequency given by *Banks* [1966] was multiplied by a "Burnside factor" of 1.3 derived from consideration of later measurements and analyses [*Burnside et al.*, 1987; *Sipler et al.*, 1991; *Pesnell et el.*, 1993; *Buonsanto et al.*, 1997]. Simulations were performed for the

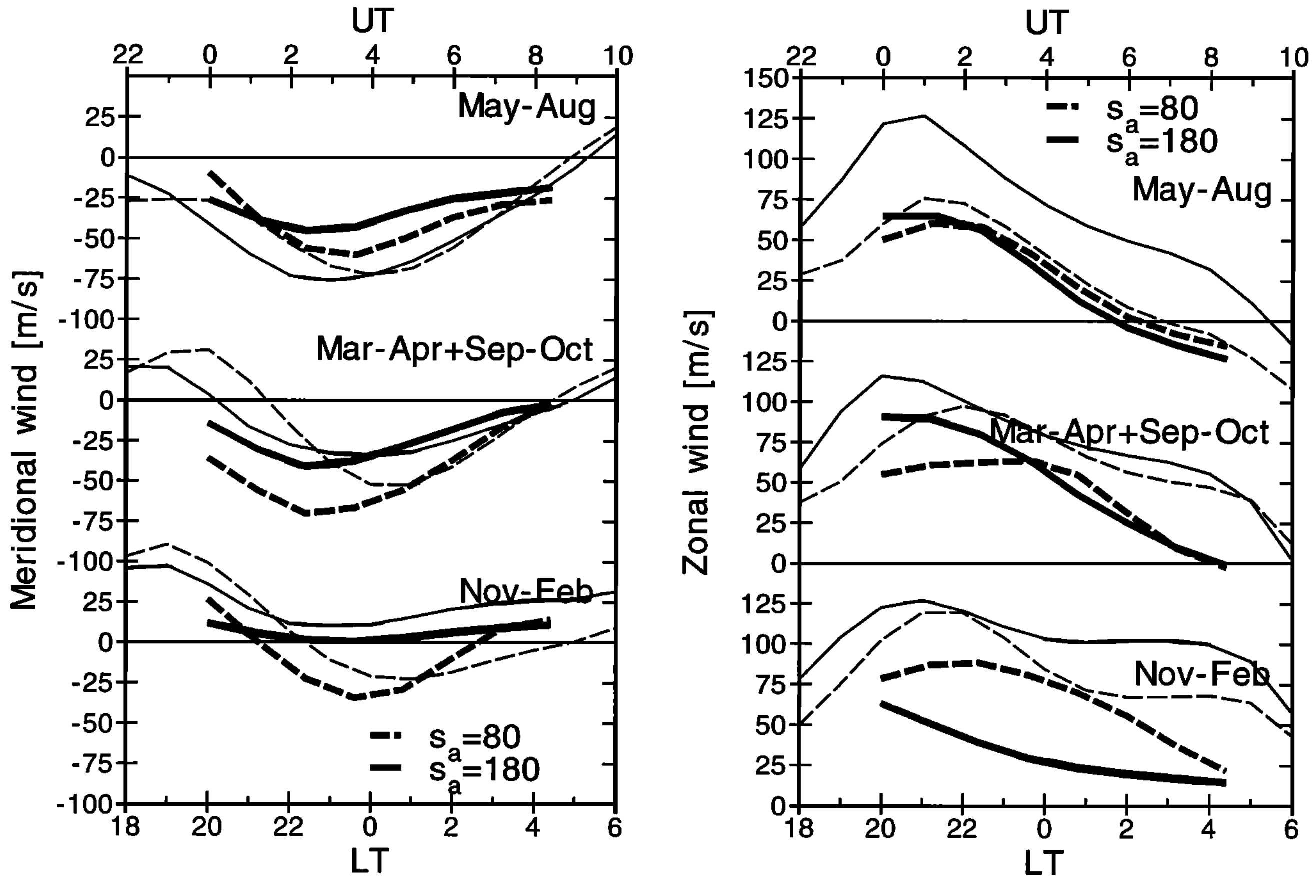

Figure 4. Arecibo thermospheric wind components at various seasons from 1980 to 1990 and $Kp \leq 3$. Heavy lines show regression analysis of the data; lighter lines, TIEGCM predictions.

months of March, June, and December to compare with observations during the equinoxes and solstices.

The model spatial resolution is 5° x 5° in latitude and longitude. Here the gridpoints closest to the geographic locations of Arequipa and Arecibo were used in the comparisons; specifically, model gridpoints at 17.5°S and 70°W were used for Arequipa and 17.5°N and 65°W for Arecibo. The altitude of the TIEGCM results was that of the median altitude of the 630 nm emission, as computed from an airglow model [*Link and Cogger,* 1988] employing mass spectrometer/incoherent scatter (MSIS) [*Hedin,* 1991] neutral temperatures and densities. This height of the emission region depends on solar activity, its centroid generally falling between 255 and 285 km.

For the three seasons, runs were made at $F_{10.7}$ values of 80, 100, 140, 180, and 210 for June and values of 80, 110, 150, 180, and 210 for March/September and December, since these values best approximated those of the observations. For each run and for each of the two locations, hourly predictions of the zonal and meridional winds at the emission height were extracted. Thus the model generated a matrix of wind predictions ordered by solar activity and local time for each location at the layer height. The TIEGCM predictions appear in the velocity *versus* time format in Figures 4, 5, and 6 and in velocity contour plots in Figures 8, 10, and 12. In both formats, linear interpolation is used to connect the discrete points of the calculations.

4. Results

During local summer in Arequipa, extensive cloud cover occurs during all or a portion of most nights; therefore we had not previously characterized the thermospheric wind behavior year by year during this season. Now, by considering only the solar flux level, we have been able to combine the data from all years for the December solstice period; however, even with this approach, for $Kp \leq 3$ there are only a modest number of nights of data. Examination of all of the data from this period indicate that there is little dependence of the winds on Kp; consequently, we have averaged the data for all values of Kp to obtain the nighttime variation of the winds for an average solar index of ~190. By inference, these results give a qualitative picture of the quiet time wind behavior for the December solstice.

The results of the bin averaging of the Arequipa data are shown in the upper portions of the upper panels in Figure 1. (The same bin averaging for $Kp \leq 3$ data yields average values similar to those in Figure 1 but with larger σ values.) For comparison, the lower panels of Figure 1 illustrate the behavior at Arecibo for the same months. In this case, the larger amounts of data permit us to use only those measurements for which $Kp \leq 3$ and $100 \leq S_a \leq 300$ to obtain the behavior at an average index of 154. The figure indicates that, as was the case for Arequipa, the thermospheric winds at Arecibo exhibit large day-to-day variations (weather),

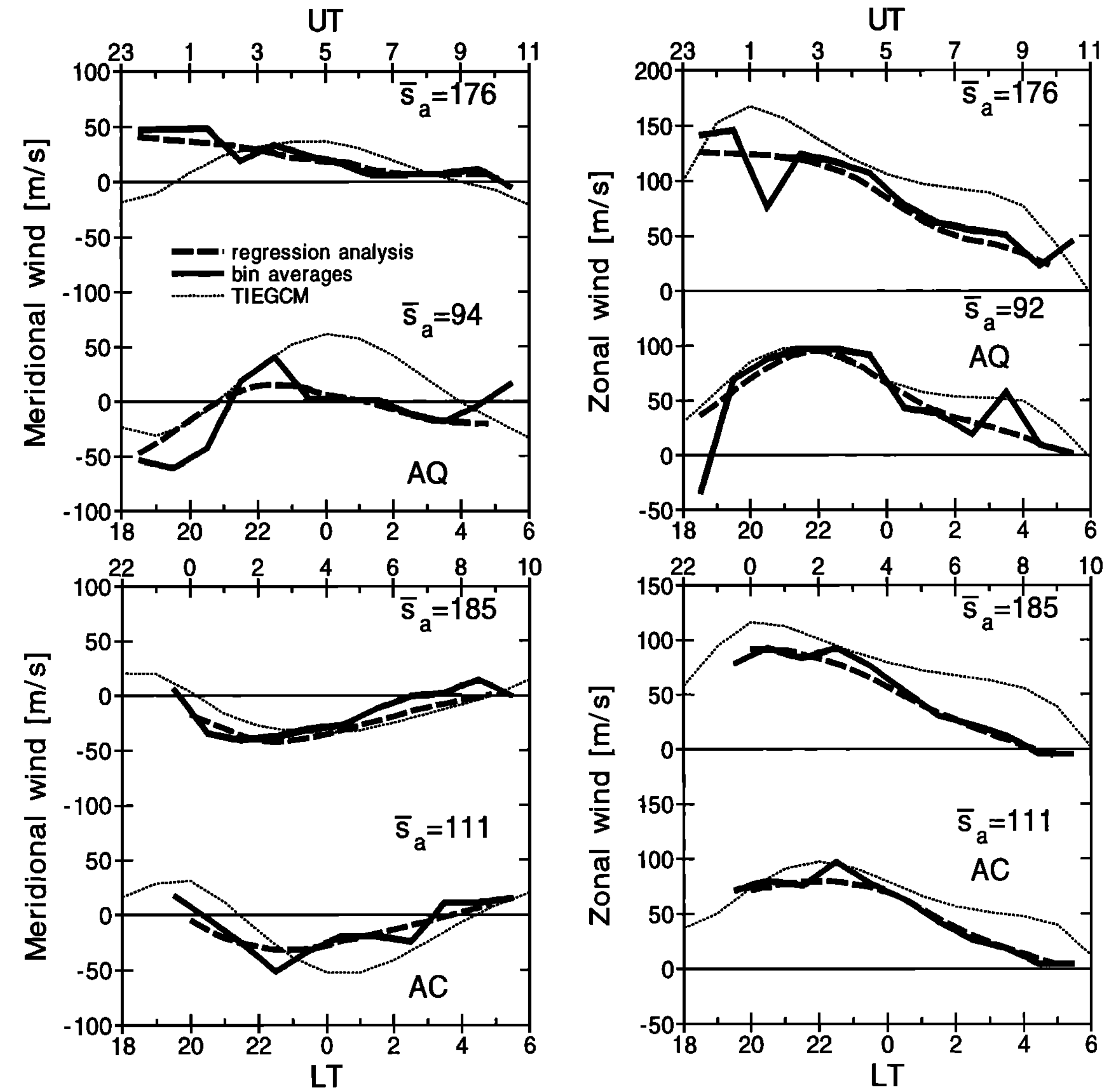

Figure 5. Thermospheric wind components at Arequipa (AQ) (upper panels) and Arecibo (AC) (lower panels) during the equinoxes (March-April + September-October), quiet conditions. Heavy solid lines show 1 hour bin averages; heavy dashed lines, regression analysis; lighter lines, TIEGCM predictions. Listed S_a are average values for bin-average curves but actual values for regression analysis curves.

necessitating averaging over many nights to discern the climate patterns.

Around the December solstice, the track of the subsolar point passes south of Arequipa, with the result that the early-night wind seen in Figure 1 is northward at ~100 m/s and dies away to small values more than 2 hours before local midnight. Throughout the night at Arecibo the meridional wind is small (<40 m/s), while the zonal winds are eastward, lessening toward zero near local dawn. At Arequipa the zonal flow velocity is approximately twice that at Arecibo (120 m/s versus 60 m/s in the early night) at all times. These differences in the magnitudes of both the meridional and the zonal wind components may result from ion-drag effects, since there are large differences in the evening and nighttime plasma density profiles over Arequipa and Arecibo, particularly during the December solstice. The consequences of these differences are considered in the Discussion section.

To provide an example of the bin-averaging techniques employed in the earlier papers, Figure 2 presents the June solstice behaviors of the winds at the two observatories, contrasting them by binning the data according to whether the solar flux values are low, $S_a \leq \sim 130$, or moderate, $\sim 130 \leq S_a \leq 300$, with the average S_a values determined by considering all of the points in the bins.

The number of data points in the average for a particular bin is shown in the top frames of Figure 2 (no average is shown for bins with fewer than 20 data points). Also, the wind component averages have been smoothed further by a weighted three-point running average, and the points have then been joined by straight-line segments. The maximum variabilities across the bins range from σ = 33 to 42 m/s at the moderate and low S_a levels. In June, Arequipa is in local winter, while Arecibo is in local summer. Again the eastward zonal winds at Arequipa are larger than at Arecibo and increase slightly with S_a value (at Arecibo there is no

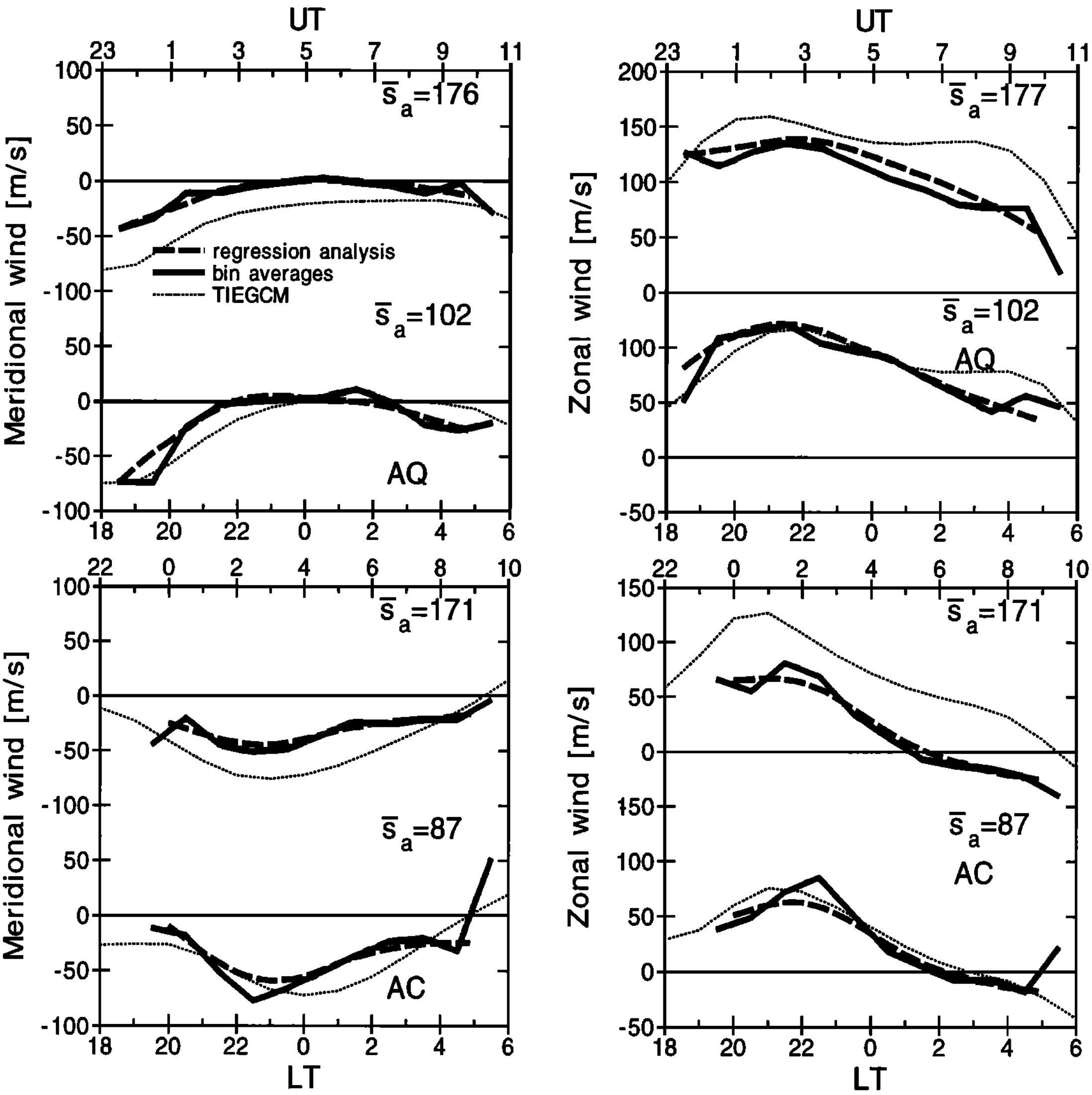

Figure 6. Thermospheric wind components during the June solstice (May - August), quiet conditions. Same format as Figure 5.

statistically significant S_a dependence). Arecibo's zonal flow reverses direction at 0200 LT, while at Arequipa the flow remains eastward. The meridional wind patterns over the two observatories, while southward or near zero throughout the night at both locations, wax and wane with time in the opposite sense.

To compare the winds at the two observatories for the same local season, we have shown the Arecibo winter data for November-February in Figure 3 for comparison with the Arequipa data of Figure 2. In Figure 3, σ does not exceed 35 m/s at both S_a levels. Now the zonal flows at both sites remain eastward throughout the night, but Arecibo's zonal winds are still smaller than those at Arequipa, with magnitudes that appear to have an inverse dependence on S_a. The meridional wind patterns, while somewhat offset from each other, now are more nearly mirror images, with poleward-equatorward-poleward transitions (Arequipa's is very weak) occurring at ~2100 and ~0200 LT. The peak-to-peak amplitudes of the meridional wind excursions are approximately the same at both sites, namely ~75 m/s at low S_a and ~50 m/s at high S_a.

Unlike Arequipa, data at Arecibo were obtained for all four seasons, providing us with an opportunity to display the year-round seasonal behavior at this site. Accordingly, we have applied the regression analysis to the Arecibo data, dividing the seasons into the two solstices and the combined equinoxes. Figure 4 displays the results in a format somewhat similar to that of Figures 2 and 3. Here, however, the heavy lines were generated by taking cuts at S_a = 80 and 180 through the velocity component contours in the S_a-t plane derived by the regression analysis. The equivalent standard error for the cuts is σ ~ 47 m/s. The lighter lines indicate predictions from the TIEGCM, which is discussed in the next section.

The results of the older bin average and the new regression analysis techniques are contrasted in Figures 5 and 6 for Arequipa and Arecibo as functions of season and solar flux. (In some of these figures the average S_a values differ for the meridional and zonal portions of the figure as a result of elimination of occasional contaminated meridional or zonal measurements.) In Figure 5, the hourly average values are indicated by the heavy solid lines (at

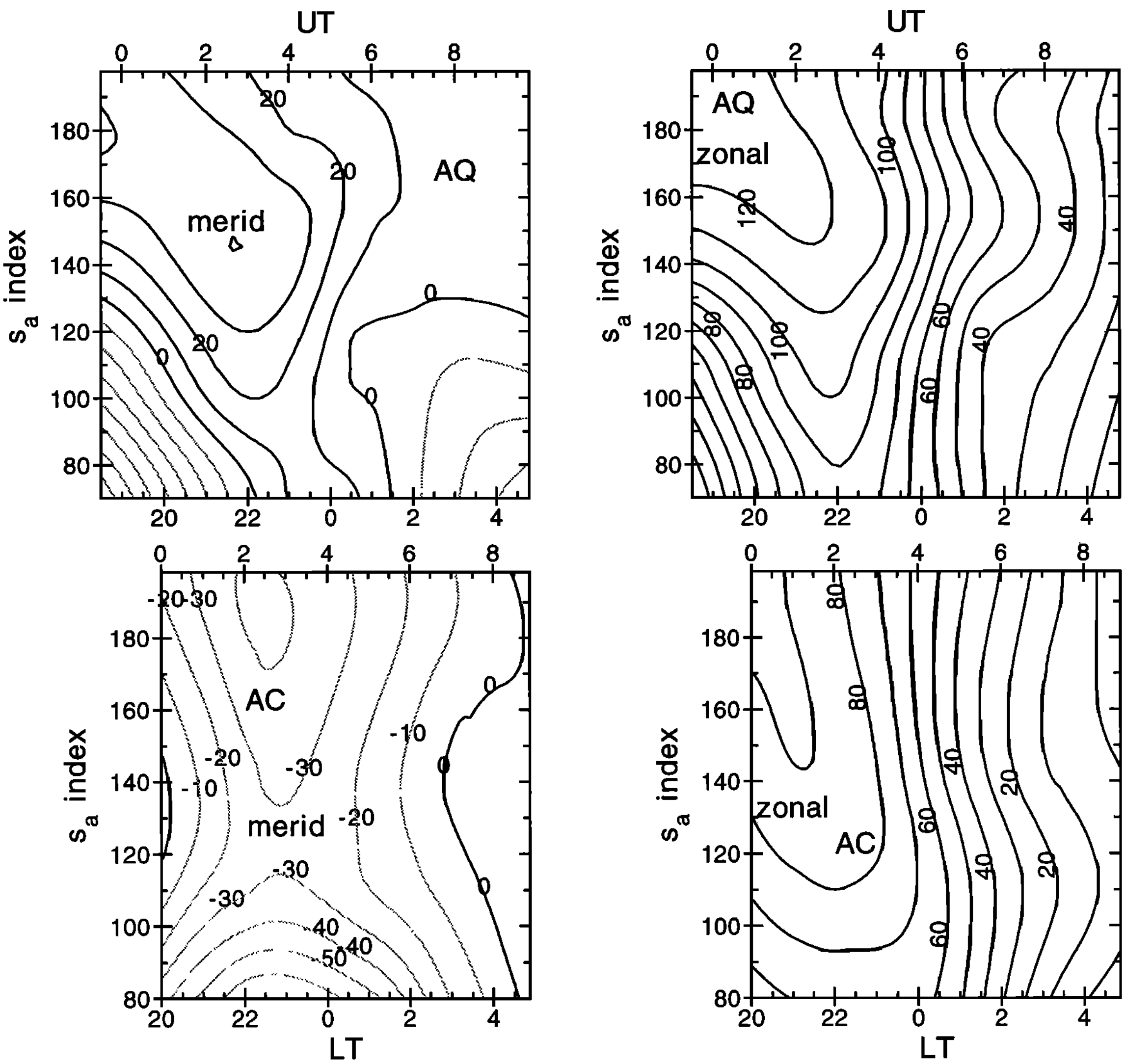

Figure 7. Thermospheric wind component contours obtained by regression analysis of the data for the equinox period (March, April, September, October data) for (upper panels) Arequipa and (lower panels) Arecibo. Dark lines represent positive velocity values; lighter lines, negative values. Contour intervals are 10 m/s.

Arequipa, σ ranges from 50 to 70 m/s for moderate to low S_a; at Arecibo, from 47 to 60 m/s). The regression analysis results are indicated by the heavy long-dashed lines, and the lighter lines are the corresponding TIEGCM predictions. In Figure 6, the format is the same as for Figure 5, and the corresponding σ values for the hourly averages range from 30 to 35 m/s (Arequipa) and from 37 to 57 m/s (Arecibo).

While the hourly average curves involve a range of S_a values whose average value is given in the figure, the cuts through the velocity contours of the regression analysis's S_a-t plane are made at precisely the stated S_a values to obtain the velocity *versus* time curves. During the equinoxes, with the subsolar point over or near the equator, the meridional winds depicted by the regression analysis curves in Figure 5 for Arequipa and Arecibo show opposite flows mirrored across the equator at both moderate (~ 180) and low (~ 100) S_a values. The zonal flows are slightly stronger at Arequipa than at Arecibo but exhibit similar temporal variations.

During the May-August solstice period, Figure 6, with the track of the subsolar point passing through or north of Arecibo, the regression analysis curves indicate a gradient in the north-south transequatorial flow. In the early night (<2000 LT), the southward flow at Arequipa is stronger than at Arecibo. After 2100 LT, the southward meridional flow from Arequipa essentially vanishes until ~ 0300 LT, while at Arecibo it strengthens, indicating a change of sign of the gradient in the trans-equatorial flow. As in the equinox observations, the temporal variations during the night are essentially opposite in shape. The eastward zonal flow at Arequipa is approximately twice as large as at Arecibo and does not exhibit the eastward-to-westward transition at ~0200 UT seen at Arecibo.

The velocity contours in the S_a-t plane generated from the regression analysis of the Arequipa and Arecibo data are displayed in Figures 7, 9, and 11. Also, the corresponding TIEGCM results are shown in the velocity contour plots of Figures 8, 10, and 12, as well as in the *v versus t* plots of Figures 4 - 6, in order to see

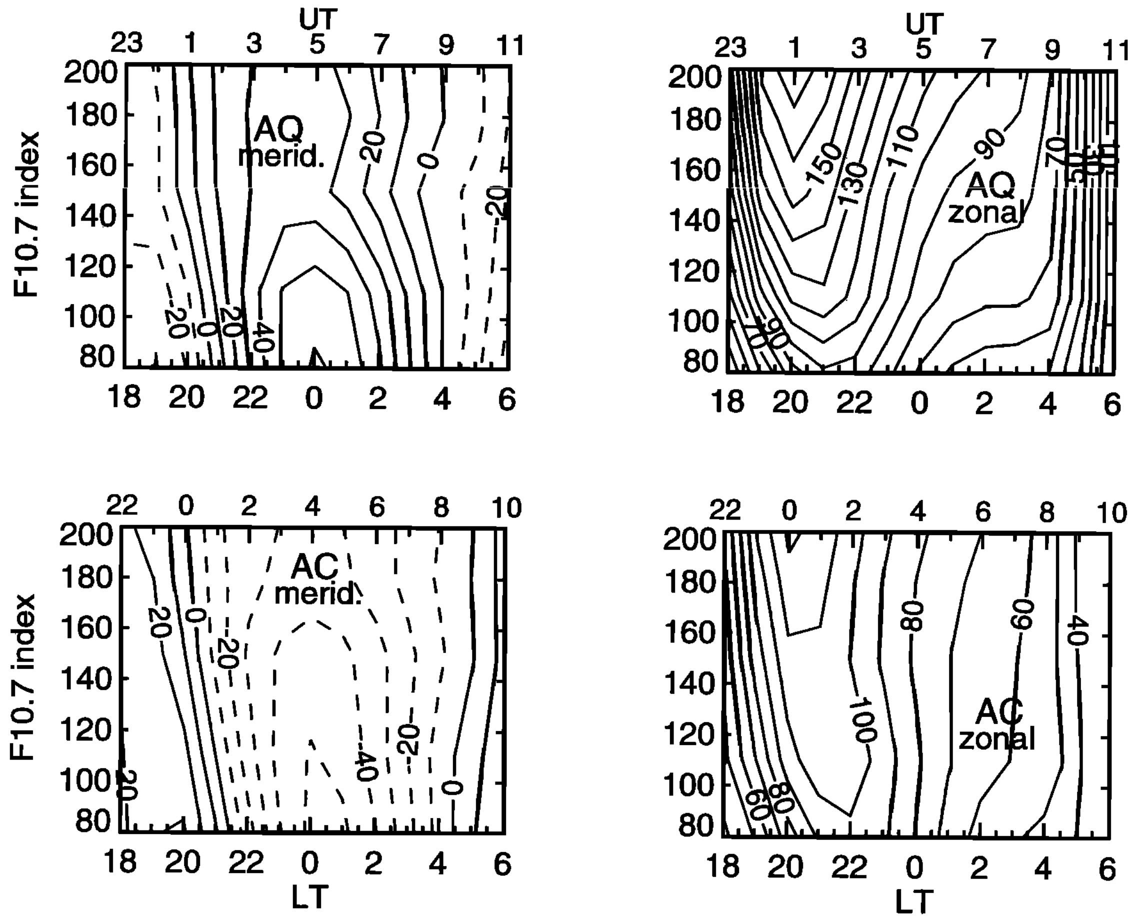

Figure 8. TIEGCM predictions of the thermospheric wind contours during the equinoxes for Arequipa (upper panels) and Arecibo (lower panels). Continuous lines represent positive velocity values; dashed lines, negative values. Contour intervals are 10 m/s.

how well an advanced ab-initio model predicts the quiet time thermosphere's behavior. The comparisons are discussed in the next section.

5. Discussion

5.1. Relative Merits of the Data Averaging Techniques

The several averaging techniques applied to the nightly wind data represent our attempt to develop better methods for removing the large day-to-day variations in the winds in order to reveal the changes in wind patterns with season and with solar EUV flux level (the climatology). The results presented in the figures permit us to compare the relative merits of the several techniques. The data analysis technique initially employed [*Biondi et al.*, 1990, 1991] involved binning all of the wind data for a given period (e.g., month/year) into 30 min intervals during the night, then determining the average value and its $\pm 1\sigma$ standard deviation for each bin. This procedure was justified by the finding [*Biondi et al.*, 1991] that, for the data points in each bin, the deviations from the mean followed a normal (Gaussian) distribution. This format of data presentation is illustrated in Figure 1 (here, 1 hour bins have been used). In the present paper, a further smoothing of the results has been achieved with a slightly modified technique which involves using a Gaussian filter to provide weighted three-point running averages of the points obtained from the original averaging, as illustrated in Figures 2 and 3.

A significant improvement in the averaging has been obtained by the use of the regression analysis technique described in section 2.2; here each of the wind data points is placed at its precise location in the S_a-t plane. In the development of the $_m v$ and $_z v$ contours in the S_a-t plane, the velocity value obtained for the n[th] point in the 50 x 50 grid at (S_a'', t'') is determined from a large number of adjacent measured values weighted inversely with their distances from the grid point. This inclusion of all of the data (a constant fraction of the total) that lie in the vicinity of a particular location in the S_a-t plane provides a more accurate description of the velocity components' time variations at particular values of S_a. The desired v *versus* t curves are obtained by taking cuts of the two-dimensional velocity contours at the desired S_a values. Thus this procedure should be an improvement over the bin-averaging methods, where the points for various nights correspond to a variety of S_a values yet are grouped within ranges of S_a values, and an appropriate average S_a value is assigned. In addition, each of the points in a given bin is weighted equally in determining the mean value for the bin, independent of the point's position within the bin.

In Figures 5 and 6 the comparisons of bin-averaging and regression analysis procedures show the latter's smoother and more reasonable representation of the nocturnal temporal variations for

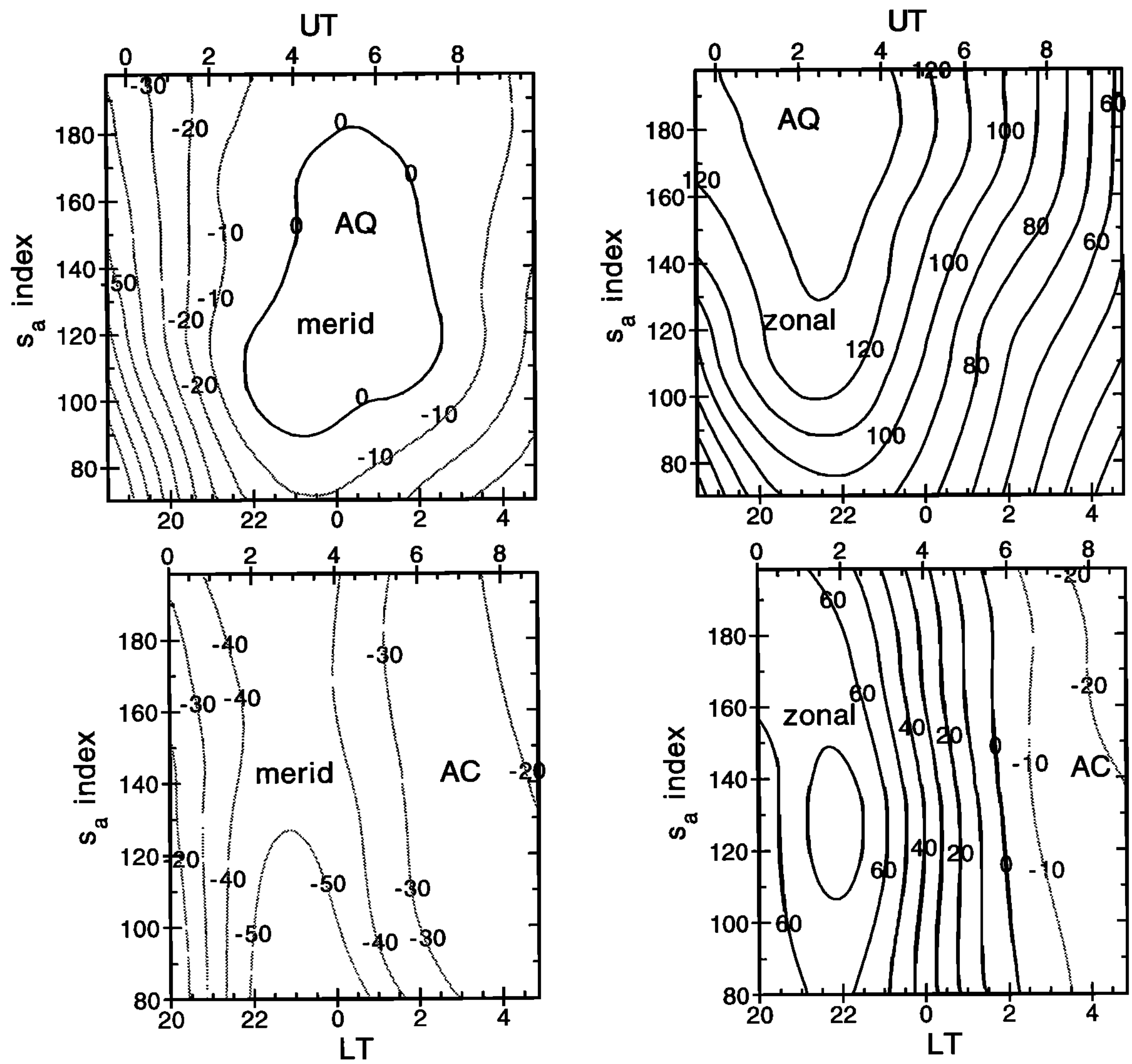

Figure 9. Wind contours obtained from the regression analysis of the measurements for the June solstice (May-August data). Same format as in Figure 7.

a given climatologic condition (season, S_a value). Although using a Gaussian filter to provide three-point running averages, as was done in Figure 2, also provides smoother curves than do the single-bin averages, the cruder weighting of the data points from the three time bins provides a poorer estimate of the wind value at a particular point in time than does the regression analysis.

5.2. Regression Analysis: TIEGCM Comparisons

Since regression analysis is the best of the several data averaging techniques that we have employed, we now compare its results for Arequipa and Arecibo with each other and against the predictions of the TIEGCM. The velocity contour plots of Figures 7 through 12 provide the fullest descriptions of measured/predicted behaviors. However, it is probably easier to first make the comparisons via *v versus t* curves at particular S_a values, as in Figures 4, 5, and 6, rather than to go directly to the wind contour plots.

In Figure 4, TIEGCM runs for Arecibo are indicated by the lighter weight lines, solid and dashed, for S_a = 180 and 80, respectively. Although the predicted wind values often differ substantially in magnitude from the observations, the general shapes of the temporal variations of both the meridional and zonal components are in rough agreement. The strongest exception occurs for the zonal winds during November - February, where the predicted postmidnight flattening of the decay is not seen, and the measurements for S_a = 180 are 1/3 to 1/4 the predicted values. In addition, the measured values exhibit a rather strong inverse dependence on S_a, opposite to both intuitive expectations and the TIEGCM predictions. The observed meridional winds often exhibit a similar inverse dependence on S_a for all seasons, as seen in the consistently stronger southward flow at low S_a, while the predicted variation with S_a is not well defined during the night, varying from direct to inverse at different times.

In an attempt to examine whether the observed zonal wind behavior at Arecibo depends on the years of data chosen for averaging, the 1980-1982 data were eliminated from the database, and the analyses rerun for the same time period, 1983-1990, used for Arequipa. With this procedure, there is little effect on the number of data points in the averages for low S_a, but for high S_a the

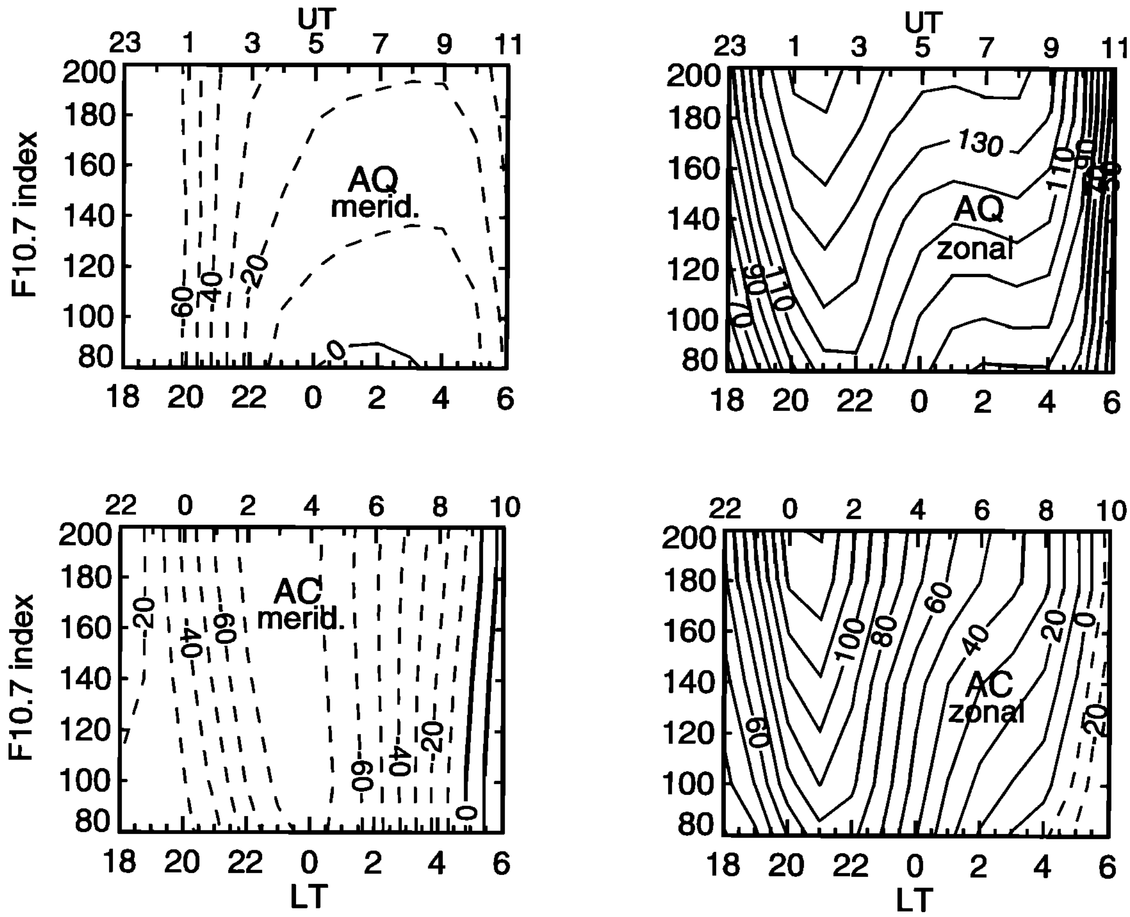

Figure 10. TIEGCM predictions of the wind contours during the June solstice. Same format as in Figure 8.

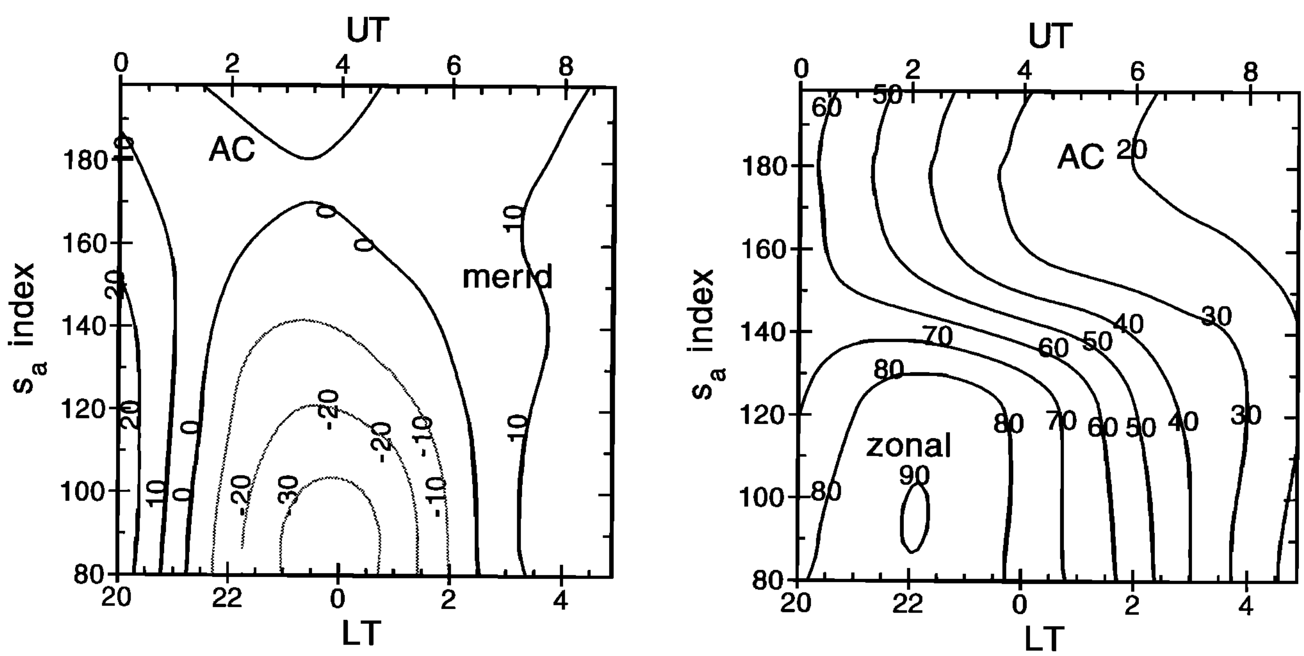

Figure 11. Wind contours obtained by regression analysis of the measurements for the December solstice (November-February data), Arecibo only. Same format as in Figure 7.

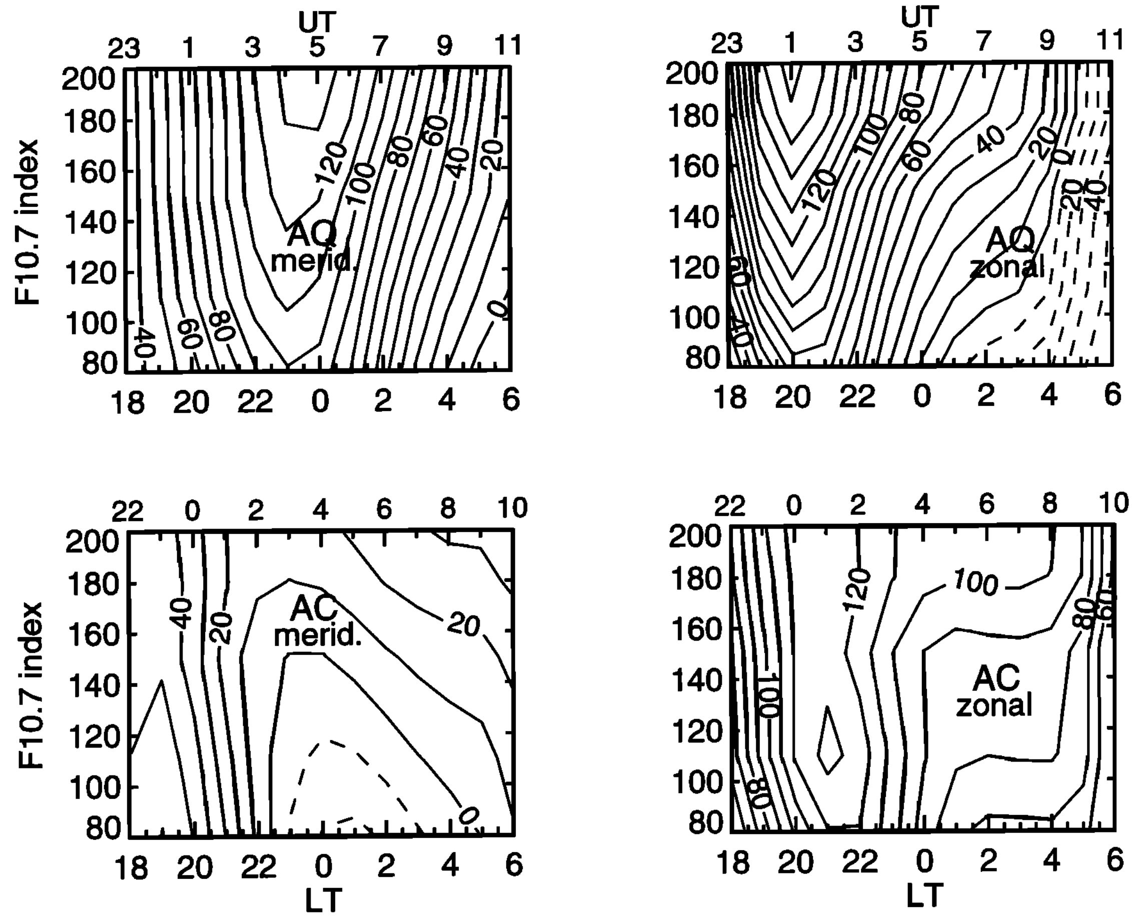

Figure 12. TIEGCM predictions of the wind contours during the December solstice. Same format as in Figure 8.

number is roughly halved, making these results less trustworthy. Both the *v versus t* curves and the wind contour plots are altered somewhat by this truncation of the Arecibo data base, but the results of the Arequipa - Arecibo comparisons described in the Results section remain essentially the same.

In the case of the November - February period, where measurements were obtained only at Arecibo, there is a reduction in the strength of the inverse dependence of the zonal winds on S_a for the truncated data set, as may be seen by comparing Figure 13 with Figure 4. However, even with the reduced data set, a direct dependence on S_a is not found, contrary to the TIEGCM predictions.

In Figures 5 and 6, ignoring the bin-average curves, we compare the regression analysis results (heavy dashed lines) with the TIEGCM predictions (light dotted lines). For the equinox, Figure 5, the measured and predicted zonal winds at Arequipa (AQ) and Arecibo (AC) agree roughly as to the temporal variations, except for the predicted flattening of the decay in the later night; however, the model values run 20-50 m/s higher than the measurements. For the meridional winds over Arequipa substantial differences are noted in the early night at S_a = 176 and at various times at both Arequipa and Arecibo for low S_a.

For the June solstice period, Figure 6, the TIEGCM predicts the shapes of the winds' temporal variations reasonably well, with the notable exception of the late night zonal wind variation at Arequipa. The predicted flattening of the decay in the postmidnight period is the most pronounced of any season, yet the observed wind speed decays smoothly. For both sites, the measured and predicted wind components differ by as much as 60 m/s during the night.

A more complete description of the measured wind behavior is given in Figures 7, 9, and 11, in which the regression analysis has been used to generate contour plots of v_m and v_z in the S_a-t plane. In the three figures the maximum equivalent standard errors are σ ~60 - 70 m/s for Arequipa and ~40 - 50 m/s for Arecibo. These velocity contour plots represent a more complete characterization of the climatological behavior of the nocturnal thermospheric winds than do the prior figures. The TIEGCM predictions, the counterparts to these observations, are shown for comparison in Figures 8, 10, and 12.

Figures 7 and 8 provide a comparison of measured and predicted behaviors at Arequipa and Arecibo around the equinoxes. As might be expected, with the subsolar point moving along the equator at equinox, the TIEGCM (Figure 8) predicts essentially mirror-image meridional flows at Arequipa and Arecibo, i.e., comparable in magnitude and equatorward in each hemisphere for much of the night, with a maximum around local midnight. The contours are consistent with solar forcing causing a daytime poleward flow that goes to zero around dusk and recommences around dawn. The model predicts that the steepness in the rise and

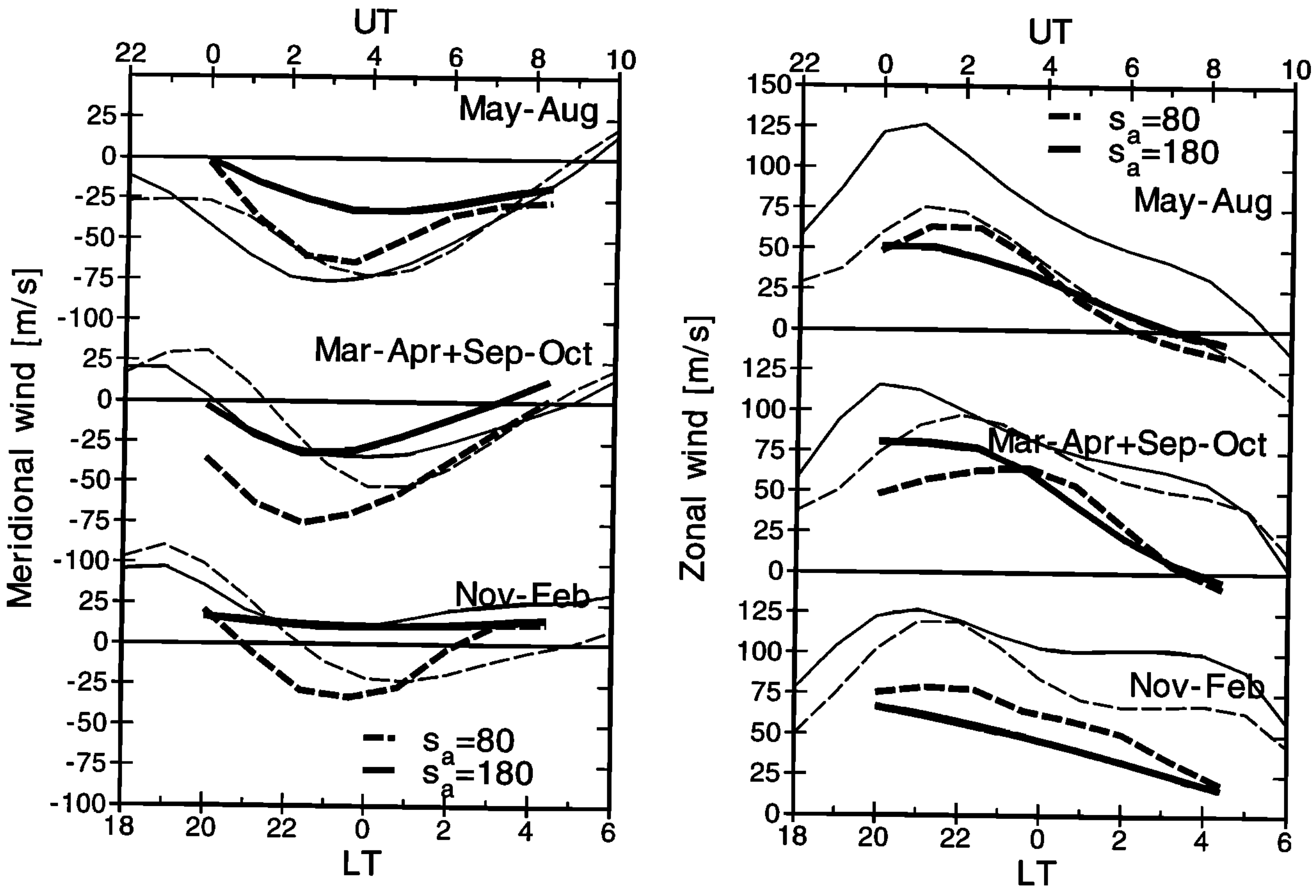

Figure 13. Arecibo thermospheric wind components for a truncated data set (1983-1990) at various seasons and $Kp \leq 3$. Heavy lines show regression analysis of the data; lighter lines, TIEGCM predictions.

fall of the velocity *versus* time curve should decrease with increasing S_a. (Note that regions of these plots where the contours are parallel to each other and vertical indicate a lack of dependence of the wind speed on S_a, i.e., the driving effect of the solar flux "saturates" for these time periods.)

The observed meridional wind behaviors at Arequipa and Arecibo (Figure 7) agree only qualitatively with predictions - the magnitudes are similar and they roughly mirror each other in flow direction, but the detailed shapes of the contours differ significantly. For low S_a values, 80 to ~120, Arequipa exhibits the TIEGCM-predicted decrease in curvature of the rise and fall in the v_m *versus* t curves with increasing S_a. However, above S_a ~140, the observed velocity contours, while roughly matching the TIEGCM's intervals, become distorted so that the rise and fall in velocity transforms to a monotonic fall at higher S_a (~170), as noted in Figure 5. In contrast, at Arecibo the measured contours are such that the rise-and-fall shape of the v_m *versus* t curves is maintained, as predicted, but the curvature does not decrease systematically with increasing S_a. The measured contours roughly mirror about a reflection line at S_a ~130, so that the v_m *versus* t curves at S_a = 100 and 180 are nearly identical, while in between, at S_a ~130, the curve is very similar in shape but shifted to smaller magnitudes by ~12 m/s.

As to the zonal wind components, for both Arequipa and Arecibo there is a better qualitative match between the TIEGCM-predicted and the observed contour shapes than was the case for the meridional components. While the absolute values of the measured/predicted winds differ, at both Arequipa and Arecibo the ranges of velocity contour values on comparable regions of the S_a-t planes are often comparable, with the TIEGCM contours running 30-40 m/s higher than the regression analysis contours. For Arequipa, as was the case for the meridional winds, the agreement between the measured (Figure 7) and predicted (Figure 8) features of the zonal wind contours becomes poorer at early times and high solar flux levels (the upper left corners of the contour plots), with the measured contours bending to the left. This has the effect of wiping out the predicted maximum in the zonal wind at 2000 LT at high S_a. At Arecibo the predicted maximum in velocity that occurs between 2000 and 2200 LT, depending on S_a, is reproduced by the measurements, but the rate of decrease in the measured velocities following the maximum is approximately twice that predicted by the TIEGCM. Both at Arequipa and Arecibo the postmidnight zonal winds show only modest alterations in speed as S_a increases, in contrast to the predicted behavior for Arequipa.

For the June solstice, Figures 9 and 10, while the detailed temporal variations differ, the measured and predicted meridional winds at Arequipa and Arecibo are southward throughout the night, with the predictions generally exceeding the measurements by ~20 - 30 m/s. At Arequipa, for all solar flux values, the winds reach a broad maximum during the night (at ~0000 LT for the measured winds, at ~0200 LT for the predicted winds). At Arecibo, both predicted and observed winds reach their maximum values at ~2300 LT.

For the zonal winds, at Arequipa both measured and predicted zonal winds are eastward throughout the night and attain comparable maximum values at ~2100 LT. The most striking difference between measured and predicted behaviors is the failure of the observations to reproduce the predicted flattening in the temporal decay of the winds between ~0000 LT and ~0400 LT for all flux values. In addition, above $S_a \sim 160$ the measured zonal winds saturate rather than continuing to increase with increasing S_a, as predicted. At Arecibo, both model and measured winds reach their maximum eastward velocities at ~2100 LT, and both reverse to a westward flow in the later night. However, while in the postmidnight period the model wind strengths continue to increase with S_a, the measured winds saturate.

For the December solstice, we have measurements only at Arecibo (Figure 11), while TIEGCM predictions have been made for both Arequipa and Arecibo (Figure 12). The measured and predicted meridional velocity contours for Arecibo are shifted slightly relative to one another in the S_a direction but are otherwise close in magnitude and similar in shape over much of the S_a-t plane. Above a critical S_a value, ~170 for measurements and ~150 for predictions, the winds remain northward throughout the night. Below these values, for both measurements and predictions, the early night northward wind changes to southward somewhat before local midnight and then changes back to northward in the postmidnight period. The measured postmidnight falloff in velocity is steeper than the TIEGCM prediction.

For the measured zonal winds, the results of Figure 11 indicate that the velocities exhibit a monotonic decrease with time throughout the night for $S_a > \sim 140$, while below $S_a \sim 120$, a rise and fall in velocity occurs, with a maximum at ~2200 LT. The TIEGCM contours (Figure 12), which extend to earlier times (1800 LT) than the measured contours, predict zonal winds that rise and fall with time at all S_a, with the maximum velocity attained at ~2100 LT.

In the discussion of Figure 4 we noted a strong, inverse dependence on S_a of the measured zonal wind speed at Arecibo compared to the direct dependence predicted by the TIEGCM. With the truncated (1983-1990) data set (Figure 13) this behavior was somewhat reduced but not eliminated. On the velocity contour plots (Figure 11), this effect is manifested over most of the S_a-t plane by measured velocity contours that run generally to lower S_a values as time increases, with the lower velocity contours lying above the higher ones. The predicted contours (Figure 12) for the period 2100-0600 LT run generally to higher S_a values as time increases, with the higher velocity contours above. Thus the inverse dependence of the strength of the zonal flow on S_a is a general feature over a wide range of observations, contradicting our intuitive expectations and the TIEGCM predictions. Possible reasons for this are discussed in the next subsection.

5.3. Ionospheric Effects

Since we deduce the thermospheric neutral winds from measurements of the Doppler shift in the nightglow OI 630 nm emission line, the properties of the F region plasma can affect our results in two ways: the distribution in altitude of the O^+/e^- concentrations determines the height of the 630 nm emission layer, and the plasma-neutral coupling (ion drag) influences the motion of the neutral thermosphere in the emission layer. At Arequipa, which is near the geomagnetic equator (small dip angle), the plasma electrodynamics leads to uplift and fall of the F layer (pre-reversal enhancement) during the course of the night. This alters (1) the altitude distribution of the 630 nm emission (produced principally by dissociative recombination of O_2^+ and e^-, the O_2^+, in turn, being produced by the $O^+ + O_2$ charge transfer reaction) and (2) the strength of the ion-neutral coupling in the emitting layer, thereby affecting the observed horizontal velocity.

Over Arecibo, where the dip angle is 50°, the height of the F layer is determined by the combined effects of the neutral meridional wind and the vertical component of the plasma drift in the plane perpendicular to the magnetic field. In this case, the electrodynamic plasma drift at a given point is determined by the neutral wind and the conductivity distribution over the entire magnetic field line passing through that point [e. g., *Fejer*, 1993]. As a result, near the December solstice, the electrodynamics of the Arecibo nighttime ionosphere is strongly controlled by the conjugate ionosphere. We conclude that for this period, when the low-latitude neutral winds and plasma drifts are strongly coupled, simply considering the season and solar flux is insufficient to fully characterize the climatological behavior of the thermospheric winds.

As to the predicted behavior, at present the model ionosphere used in the TIEGCM appears to be insufficiently "tuned," consistently yielding underestimates of the ion densities. The consequent too-small ion drag on the neutral thermosphere may account in part for model zonal winds that are larger than observations. Current efforts to validate the model ionosphere are discussed in a forthcoming paper (*G. Crowley et al.*, Validation of the NCAR-TIEGCM for equinox solar minimum conditions, submitted to *Journal of Geophysical Research*, 1999). Also, changes in model inputs being considered by NCAR include modifications of the tidal amplitudes at 100 km altitude and reduction of the E region electron densities, both of which will lead to altered coupling effects between the E and F regions.

5.4. Geomagnetically Quiet Conditions

In this work we have used the "current" *Kp* values to select geomagnetically quiet conditions. However, as pointed out in numerous studies [e.g., *Fejer and Scherliess*, 1997], the nature of the equatorial ionosphere is strongly dependent on the history of the geomagnetic activity for up to 30 hours earlier. Since use of this more stringent criterion would have significantly decreased the number of wind measurements that could be used in the database and since we have no a priori means of determining the length of this period for a given observation night, we have adopted the simpler "current" criterion.

5.5. Comparison With DE-2 Satellite Results

Around solar maximum, during the premidnight period there is an apparent, 20-30 m/s difference between the zonal thermospheric wind determinations by the Arequipa FPI and by the DE-2 satellite [*Wharton et al.*, 1984]. The peak zonal winds occurred at ~2100 LT, with the ground-based observations yielding values of ~120-135 m/s and the satellite ~150-165 m/s. Due to the pre-reversal enhancement, the F region ionosphere is very high, causing the 630 nm nightglow to be very weak. This follows from the fact that the 630 nm radiation is produced by dissociative recombination of ionospheric electrons with O_2^+ ions, and the O_2^+ concentration decreases sharply with altitude, mirroring the falloff with altitude of O_2, necessary for O_2^+ production through the $O^+ + O_2$ charge transfer reaction. As a result, the DE-2's FPI instrument did not provide thermospheric wind determinations, and instead the WATS mass spectrometer instrument was used to determine an in situ zonal wind in the 300-400 km altitude region.

It should be noted that, even at the maximum solar flux value for these studies, $S_a = 200$, after 2100 LT the median emission altitude of the 630 nm radiation remains below 300 km [see *Meriwether et al.*, 1997, Figure 2b]. The ground-based Arequipa FPI looking up through this region obtained some wind measurements but not during during strong pre-reversal enhancements (weakest 630 nm airglow), so that its database for the early night was limited, and the resulting averages are probably somewhat biased.

The Jicamarca radar's nighttime plasma drift measurements, which for this period were around the F region peak [*Fejer et al.*, 1991], support DE-2's zonal neutral winds. For our part, having reexamined our data acquisition and the subsequent analysis to deduce the wind values [*Biondi et al.*, 1990, 1991], we find no reason to doubt the absolute values given in the present paper, but consideration must be taken of the quoted uncertainties. In view of the different altitudes under observation by DE-2 and the Arequipa FPI, an alternate explanation of the difference in zonal wind values is that there is a modest altitude gradient in the neutral thermosphere's zonal winds in the 250 - 400 km region.

6. Conclusions

In treating the thermospheric wind data to determine climatological behaviors of the winds as functions of season, solar activity, and time during the night, the multivariate regression analysis improves on our previous method of averaging data that is binned simply by month/year, average S_a, and time during the night. Being more flexible than binning, the local regression method provides a better representation of how the winds vary with local time and solar activity without distorting the average behavior, as do spline fits.

A number of points have emerged in the presentation of the regression analysis results and in their discussion. In the intercomparison of the observed Arequipa and Arecibo thermospheric winds there are areas of qualitative agreement as to the expected behavior at the two sites for geomagnetically quiet periods. That is, they are consistent with a principal driving force for the winds arising from the strength and the location of the absorbed solar EUV flux in the upper atmosphere. There are, however, periods when considerable departures from this behavior are observed. These effects most probably arise from an omitted factor: the very different ion drag effects at the two sites, arising from differences in the strength and behavior of the F region plasma at the 630 nm emission height over Arequipa and Arecibo. At present, we are unable to parameterize the ion drag in any reasonable way for ordering the data further; there are simply too many variable factors in determining the F region ionosphere's strength and dynamics.

In comparisons of the measured winds at both sites with the TIEGCM predictions, there are also areas of qualitative agreement and of striking differences. Here, however, the model includes electrodynamic considerations in an attempt to describe the effects on the thermospheric neutral wind of vertical motions and horizontal drifts of the ionosphere. While these electrodynamics additions to the TIEGCM may be incomplete, they are a step beyond what we have been able to do with the measurements in fully characterizing the quiet time winds.

The extensive observations from Arequipa and Arecibo represent one of the most complete data sets on low-latitude thermospheric winds, permitting an initial determination at these two low-latitude sites of the wind climatology under geomagnetically quiet conditions. Also, it has been possible to compare the measurements with predictions from the current, state-of-the-art TIEGCM model.

While Arecibo thermospheric wind determinations are no longer made routinely, the Arequipa database continues to be augmented by ongoing, nearly continuous observations. Therefore at Arequipa we may expect further improvements in the description of the quiet time climatology and possibly extension to an examination of changes that occur under geomagnetically disturbed conditions (where an even larger database is required).

Acknowledgments. The authors are greatly indebted to C. A. Tepley and the late R. G. Burnside for having made available to us their Arecibo thermospheric wind database for analysis, the results of which have been included in this paper. The material reported in this paper is based on work supported by the National Science Foundation under grants ATM-9414403 at the University of Pittsburgh, ATM-9731704 at Utah State University, ATM-9714770 at Clemson University and ATM-976035 and ATM-970636 at the University of Texas (Dallas).

Janet G. Luhmann thanks Roger Smith and Dwight Sipler for their assistance in evaluating this paper.

References

Banks, P., Collision frequencies and energy transfer: Ions, *Planet. Space Sci.*, *14*, 1105, 1966.

Biondi, M.A., and D.P. Sipler, Horizontal and vertical winds and temperatures in the equatorial thermosphere: Measurements from Natal, Brazil during August-September 1982, *Planet. Space Sci.*, *33*, 817-823, 1985.

Biondi, M.A., and J.W. Meriwether, Measured response of the equatorial thermospheric temperature to geomagnetic and solar flux changes, *Geophys. Res. Lett.*, *12*, 267, 1985.

Biondi, M.A., J.W. Meriwether, B.G. Fejer, and S.A. Gonzales, Seasonal variations in the equatorial thermospheric wind at Arequipa, Peru, *J. Geophys. Res.*, *95*, 12243-12250, 1990. (Correction, *J. Geophys. Res.*, *100*, 7863, 1995.)

Biondi, M.A., J.W. Meriwether, B.G. Fejer, S.A. Gonzales, and D.C. Hallenbeck, Equatorial thermospheric wind changes during the solar cycle: Measurements from Arequipa, Peru from 1983 to 1990, *J Geophys. Res.*, *96*, 15917-15930, 1991. (Correction, *J. Geophys. Res.*, *100*, 7863, 1995.)

Buonsanto, M. J., D. P. Sipler, G. B. Davenport, and J. M. Holt, Estimation of the O^+,O collision frequency from coincident radar and Fabry Perot observations at Millstone Hill, *J. Geophys. Res.*, *102*, 17267-17274, 1997.

Burnside, R.G., F.A. Herrero, J.W. Meriwether, and J.C.G. Walker, Optical observations of thermospheric dynamics at Arecibo, *J. Geophys. Res.*, *86*, 5532-5540, 1981.

Burnside, R. G., C. A. Tepley, and V. B. Wickwar, The O^+ O collision cross section: Can it be inferred from aeronomical measurements?, *Ann. Geophys.*, *5*, 343, 1987.

Cleveland, W.S., Robust, locally weighted regression and smoothing scatterplots, *J. Am. Stat. Assoc.*, *74*, 829-836, 1979.

Cleveland, W.S. and S.J. Devlin, Locally-weighted regression: approach to regression analysis by local fitting, *J. Am. Stat. Assoc.*, *83*, 596-610, 1988.

Cleveland, W.S., S.J. Devlin, and E. Grosse, Regression by local fitting: methods, properties, and computational algorithms, *J. Econometrics*, *37*, 87-114, 1988.

Fejer, B G., F-region plasma drifts over Arecibo Solar cycle, seasonal, and magnetic activity effects, *J Geophys Res.*, *98*, 13645-13652, 1993.

Fejer, B G, The electrodynamics of the low-latitude ionosphere· Recent results and future challenges, *J. Atmos. Sol. Terr Phys*, *59*, 1465-1482, 1997

Fejer, B. G, and L Scherliess, Empirical models of storm time equatorial zonal electric fields, *J. Geophys. Res.*, *102*, 24047-24056, 1997

Fejer, B. G, E. R de Paula, S. A. Gonzales, and R. F. Woodman, Average vertical and F-region zonal plasma drifts over Jicamarca, *J. Geophys. Res.*, *96*, 13901-13906, 1991.

Hedin, A. E., Extension of the MSIS thermospheric model into the middle and lower atmosphere, *J Geophys Res.*, *96*, 1159-1172,1991.

Hedin, A E., N. W. Spencer, and T. L Killeen, Empirical global model of upper thermospheric winds based on Atmosphere and Dynamics Explorer satellite data, *J. Geophys. Res.*, *93*, 9959-9978, 1988

Hedin, A. E., et al., Revised global model of thermosphere winds using satellite and ground based observations, *J. Geophys. Res.*, *96*, 7657-7688, 1991.

Link, R. and L. L. Cogger, A reexamination of the OI 6300 Å nightglow, *J. Geophys. Res.*, *93*, 9883-9892, 1988. (Correction, *J. Geophys. Res.*, *94*, 1556, 1989.)

Meriwether, J.W., and M. A. Biondi, Optical interferometer observations of 630-nm intensities, thermospheric winds and temperatures near the geomagnetic equator, *Adv. Space Res.*, *15(5)*, 17-26, 1995.

Meriwether, J.W., M. A. Biondi, and D. N. Anderson, Equatorial airglow depletions induced by thermospheric winds, *Geophys. Res. Lett.*, *12*, 487-490. 1985.

Meriwether, J.W., J. W. Moody, M. A. Biondi, and R. G. Roble, Optical interferometric measurements of nighttime equatorial thermospheric winds at Arequipa, Peru, *J. Geophys. Res.*, *91*, 5557-5560, 1986.

Meriwether, J. W., J. L. Mirick, M. A. Biondi, F. A. Herrero, and C. G. Fesen, Evidence for orographic wave heating in the equatorial thermosphere at solar maximum, *Geophys. Res. Lett.*, *23*, 2177-2180, 1996.

Meriwether, J. W., M. A. Biondi, F. A. Herrero, C. G. Fesen, and D. C. Hallenback, Optical interferometric studies of the nighttime equatorial thermosphere: Enhanced temperatures and zonal wind gradients, *J. Geophys. Res.*, *102*, 20041-20058, 1997.

Pesnell, W. D., K. Omidvar, and W R. Hoegy, Momentum transfer collision frequency of O^+ - O, *Geophys. Res. Lett.*, *20*, 1343-1346, 1993.

Richmond, A. D., E. C. Ridley, and R. G. Roble, A thermosphere-ionosphere general circulation model with coupled electrodynamics, *Geophys. Res Lett.*, *19*, 601-604, 1992

Sipler, D. P., M E. Hagan, M E. Zipf, and M. A. Biondi, Combined optical and radar wind measurements in the F region over Millstone Hill, *J Geophys Res.*, *96*, 21255-21262, 1991.

Wharton, L. E , N. W. Spencer, and H C Mayr, The earth's thermospheric superrotation from Dynamics Explorer 2, *Geophys Res Lett.*, *11*, 531-534, 1984.

M A. Biondi, Department of Physics and Astronomy, University of Pittsburgh, Pittsburgh, PA 15260.

B.G Fejer and S Y. Sazykin, CASS, Utah State University, Logan, UT 84322-4405

C G. Fesen, W B Hanson Center for Space Sciences, University of Texas (Dallas), Richardson, TX 75083-0688.

J.W Meriwether, Department of Physics and Astronomy, Clemson University, Clemson, SC 29634-1911.

(Received December 17, 1998; revised March 1, 1999; accepted April 5, 1999 .)